ACCOUNTS of chemical research

Article

pubs.acs.org/accounts

Electronic Doping and Redox-Potential Tuning in Colloidal Semiconductor Nanocrystals

Alina M. Schimpf, Kathryn E. Knowles, Gerard M. Carroll, and Daniel R. Gamelin*

Department of Chemistry, University of Washington, Seattle, Washington 98195-1700, United States

CONSPECTUS: Electronic doping is one of the most important experimental capabilities in all of semiconductor research and technology. Through electronic doping, insulating materials can be made conductive, opening doors to the formation of *p*−*n* junctions and other workhorses of modern semiconductor electronics. Recent interest in exploiting the unique physical and photophysical properties of colloidal semiconductor nanocrystals for revolutionary new device technologies has stimulated efforts to prepare electronically doped colloidal semiconductor nanocrystals with the same control as available in the corresponding bulk materials. Despite the impact that success in this endeavor would have, the development of general and reliable methods for electronic doping of colloidal semiconductor nanocrystals remains a long-standing challenge. In this Account, we review recent progress in the development and characterization of electronically doped colloidal semiconductor nanocrystals. Several successful methods for introducing excess band-like charge carriers are illustrated and discussed, including photodoping, outer-sphere electron transfer, defect doping, and electrochemical oxidation or reduction. A distinction is made between methods that yield excess band-like carriers at thermal equilibrium and those that inject excess charge carriers under thermal nonequilibrium conditions (steady state). Spectroscopic signatures of such excess carriers, accessible by both equilibrium and nonequilibrium methods, are reviewed and illustrated. A distinction is also proposed between the phenomena of electronic doping and redox-potential shifting. Electronically doped semiconductor nanocrystals possess excess band-like charge carriers at thermal equilibrium, whereas redox-potential shifting affects the potentials at which charge carriers are injected under nonequilibrium conditions, without necessarily introducing band-like charge carriers at equilibrium. Detection of the key spectroscopic signatures of band-like carriers allows distinction between these two regimes. Both electronic doping and redox-potential shifting can be powerful tools for tuning the performance of nanocrystals in electronic devices. Finally, key chemical challenges associated with nanocrystal electronic doping are briefly discussed. These challenges are centered largely on the availability of charge-carrier reservoirs with suitable redox potentials and on the relatively poor control over nanocrystal surface traps. In most cases, the Fermi levels of colloidal nanocrystals are defined by the redox properties of their surface traps. Control over nanocrystal surface chemistries is therefore essential to the development of general and reliable strategies for electronically doping colloidal semiconductor nanocrystals. Overall, recent progress in this area portends exciting future advances in controlling nanocrystal compositions, surface chemistries, redox potentials, and charge states to yield new classes of electronic nanomaterials with attractive physical properties and the potential to stimulate unprecedented new semiconductor technologies.

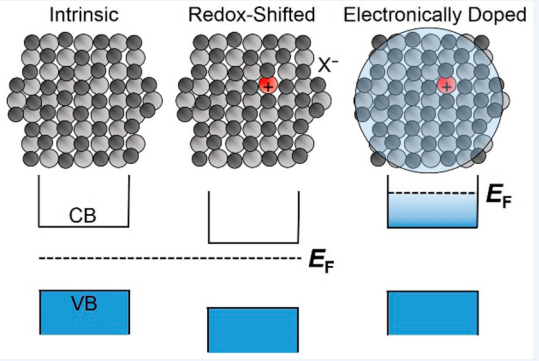

1. INTRODUCTION

The richly tunable chemical and physical properties of colloidal semiconductor nanocrystals, in conjunction with their flexible surface functionalization, solubility, and processability, make this class of materials exceptionally attractive for both fundamental and applied sciences. Unprecedented physical properties have been achieved in semiconductor nanocrystals via control of size, shape, composition, and heterointerfacing. A major remaining challenge pertains to electronic doping of nanocrystals. Electronic doping is one of the most important experimental capabilities in semiconductor physics, allowing transformation of insulators into conductive materials and thereby enabling the formation of transistors, diodes, and other key building blocks of semiconductor electronics. Although many proposed nanocrystal applications rely on charge transport, electronic doping of colloidal semiconductor nanocrystals and control over the resulting concentrations of band-like electrons or holes have proven extraordinarily challenging. These challenges have both synthetic and electronic-structure components and are intimately intertwined with nanocrystal surface chemistry, which is arguably the least understood and least controllable aspect of colloidal nanocrystal chemistries.

In this Account, we review recent progress toward nanocrystal electronic doping. We outline the basic physical properties that have emerged as signatures of electronically doped semiconductor nanocrystals and describe their origins. We propose that a distinction between nanocrystal electronic doping and redox-potential tuning is helpful for organizing and interpreting observations from recent literature.

Received: April 6, 2015
Published: June 29, 2015

DOI: 10.1021/acs.accounts.5b00181
Acc. Chem. Res. 2015, 48, 1929−1937

Scheme 1

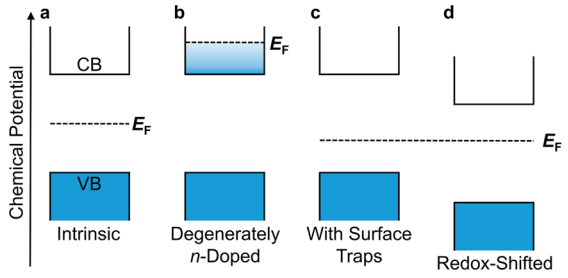

1.1. Electronic Doping

Intrinsic semiconductors have their Fermi level (E_F) located in the middle of the bandgap (Scheme 1a).[1] Typically, discussions of nanocrystal electronic doping describe shifting the Fermi level beyond a band edge to introduce delocalized electrons (*n*-doping, Scheme 1b) or holes (*p*-doping). Semiconductors with E_F positioned within a band (Scheme 1b) are degenerately doped, and their free carrier concentrations do not change with temperature. An example is photodoped ZnO nanocrystals, which show a constant number of delocalized electrons between room and liquid-helium temperatures.[2,3] Nondegenerately doped semiconductors have E_F within thermal reach of a band edge such that the band is thermally populated with charge carriers. A signature of this regime is carrier freeze-out, in which carriers localize at low temperatures. An example of nondegenerately doped colloidal nanocrystals is *n*-doped TiO_2, which shows characteristics of both localized and delocalized electrons that vary with temperature.[4−7] Many colloidal nanocrystals possess donor or acceptor defects, for example, at their surfaces, that define E_F (Scheme 1c). In many nanocrystals, surface traps reside deep within the gap and the resulting free-carrier concentration is negligible at or around room temperature, similar to intrinsic semiconductors.

Equation 1 presents a concise summary of the above descriptions of electronic doping. Here, N is the free-carrier density. Only when E_F is near or within a band does a change in E_F change N by a significant amount. In solution, E_F can be equated with redox potential (or carrier chemical potential)[8] and, for individual nanocrystals, ∂N corresponds to a quantized change in the number of delocalized electrons or holes. Equation 1 therefore equivalently states that electronically doped nanocrystals show a change in the number of band-like carriers with a change in carrier chemical potential.

$$\frac{\partial N}{\partial E_F} \neq 0 \tag{1}$$

1.2. Redox-Potential Tuning

In molecules, structural perturbations commonly shift redox potentials without changing the molecule's oxidation state. Analogous redox-potential tuning ("redox shifting") can also occur in semiconductor nanocrystals, in which nanocrystal band-edge potentials shift relative to E_F without introducing a significant number of free carriers at equilibrium (Scheme 1d). Although in some cases accompanied by equilibrium injection of band-like charge carriers, redox shifting can also strongly affect nanocrystal electronic properties relevant to device applications, redox reactivities, and spectroscopy even without introducing free carriers. We propose that by distinguishing between perturbations that introduce free carriers and those that only shift redox potentials, it is possible to reconcile many observations from recent literature and gain deeper insight into the fundamental synthetic challenges and physical properties associated with electronically doped nanocrystals.

2. SPECTROSCOPIC SIGNATURES OF EXCESS BAND-LIKE CHARGE CARRIERS

Like in molecules, oxidation or reduction alters a variety of nanocrystal physical properties that can be addressed in solution without electrical contact. We begin by describing the spectroscopic signatures of excess band-like charge carriers in colloidal semiconductor nanocrystals.

2.1. Electronic Absorption Spectroscopy

Excess band-like charge carriers generate two primary spectroscopic signatures: (i) a bleached band-edge absorption and (ii) a comparably intense infrared (IR) intraband absorption. Figure 1 illustrates these signatures for *n*-doped colloidal CdSe nanocrystals.[9] The data in Figure 1 show CdSe nanocrystals with an average number of excess electrons per nanocrystal ($\langle n_e \rangle$) of up to 1, quantified by independent chemical titration, placing E_F above the conduction-band (CB) edge (Scheme 1b). The origins of the spectroscopic changes are illustrated schematically in the inset of Figure 1: Excess CB electrons block the lowest-energy interband transitions, causing the band-edge bleach (middle). These new electrons can also be excited to higher CB levels, causing the new IR absorption. The lower panel plots the normalized absorption difference at $\langle n_e \rangle = 1$. The first excitonic absorption is 50% bleached when the first CB orbital is half filled, illustrating use of this bleach to quantify *n*-doping.[10] With accumulation to large carrier

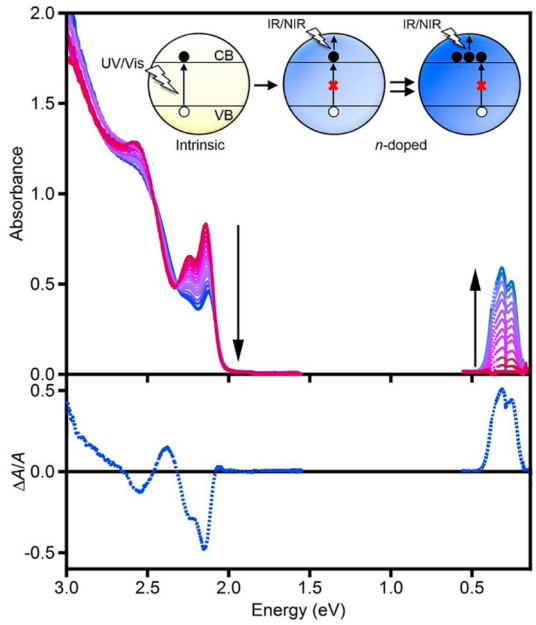

Figure 1. Spectroscopic signatures of excess band-like charge carriers in colloidal semiconductor nanocrystals. The addition of CB electrons to d = 3.8 nm CdSe nanocrystals bleaches band-edge absorption and introduces new IR intraband absorption. (top) Visible and IR absorption as a function of photodoping level. The arrows show increased electron accumulation up to $\langle n_e \rangle = 1$. (bottom) Normalized absorption difference $(\Delta A/A = (A_{doped} - A_{undoped})/A^{max}_{undoped})$ at $\langle n_e \rangle = 1$ ($\langle N_e \rangle = 3.5 \times 10^{19}$ cm^{-3}). The inset illustrates the origins of these spectroscopic signatures. Adapted with permission from ref 9. Copyright 2013 American Chemical Society.

DOI: 10.1021/acs.accounts.5b00181
Acc. Chem. Res. 2015, 48, 1929−1937

densities, these IR absorption bands evolve into localized surface plasmon resonances.[3,11−23]

The aforementioned spectroscopic signatures are nicely illustrated through spectroelectrochemistry on films of PbSe nanocrystals.[24] Figure 2a plots normalized differential absorption ($\Delta A/A$) spectra of PbSe nanocrystals measured under bias. As in Figure 1, both a band-edge bleach (~0.6 eV) and intraband absorption (~0.2 eV) are observed under negative bias. Remarkably similar spectral changes are also observed under positive bias, indicating the rare ability to add excess band-like carriers of either type. The spectroscopic signatures of *n*- and *p*-doping are nearly identical owing to the similar CB and valence-band (VB) structures of PbSe. Figure 2b plots the excitonic absorption bleach vs applied potential. For both negative and positive bias, the bleach increases and then levels off with increasing potential. Figure 2c illustrates the experiment schematically. With applied bias, E_F can be tuned relative to the nanocrystal band edges. When E_F is above the CB edge (approximately −0.5 V vs Ag pseudoreference) or below the VB edge (~0.0 V vs Ag), a steady-state (nonequilibrium) concentration of free carriers is established within the nanocrystals until the bias is removed. Although the number of excess carriers per nanocrystal was not quantified, the first exciton should be fully bleached at eight carriers per nanocrystal because of the 8-fold degeneracies of the PbSe CB and VB edges.[25] Injection of both carrier types has also been observed in the spectroelectrochemistry of HgTe nanocrystal films.[26]

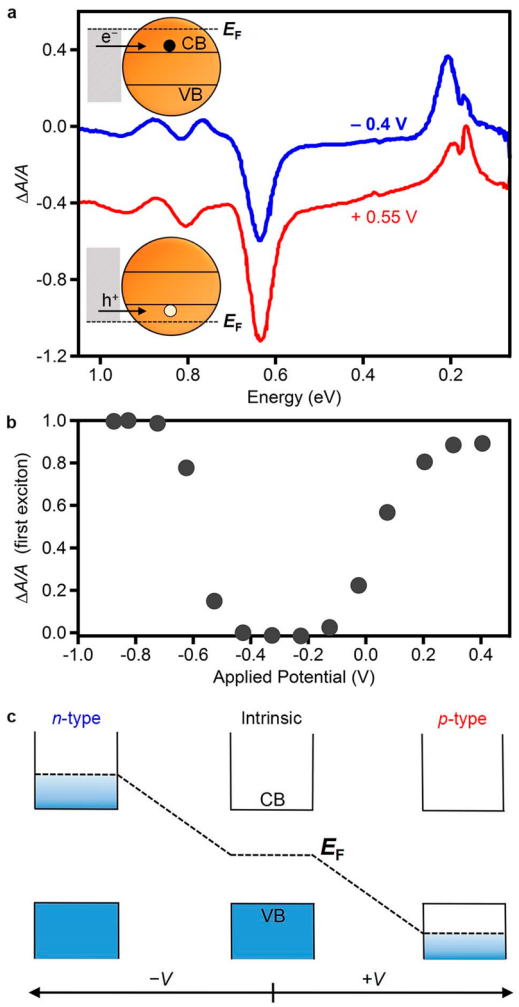

Figure 2. Electrochemical addition of excess band-like charge carriers to colloidal PbSe nanocrystals. (a) Normalized differential absorption spectra collected at positive and negative applied potentials, referenced to Ag wire. Negative bias causes nanocrystal reduction (blue) and positive bias causes nanocrystal oxidation (red). (b) First exciton bleach as a function of applied potential. Panels a and b adapted with permission from ref 24. Copyright 2003 American Chemical Society. (c) Schematic representation of the shift in E_F with applied potential.

2.2. Carrier Dynamics and EPR

In addition to changing the absorption spectrum, excess carriers commonly introduce new nonradiative relaxation pathways that shorten photoluminescence decay times and decrease luminescence quantum yields. Figure 3a shows photoluminescence decay curves measured for colloidal CdSe and photodoped *n*-type CdSe nanocrystals prepared as in Figure 1. An increase in photoluminescence intensity at short times is observed upon photodoping, arising from the negative trion's enhanced radiative-recombination rate. A new fast-decay component is also observed, corresponding to trion Auger recombination. Such changes in carrier dynamics are strong indicators of successful electronic doping.

In some cases, excess charge carriers have been identified using electron paramagnetic resonance (EPR) spectroscopies. Figure 3b shows EPR spectra and *g* values for various colloidal

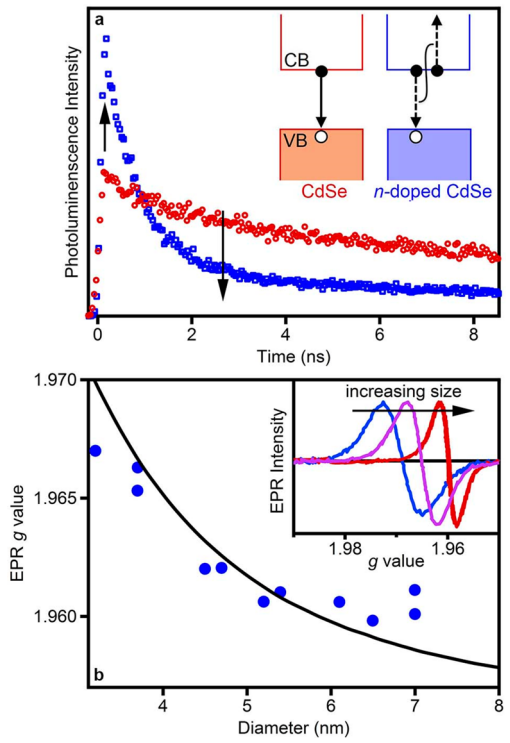

Figure 3. Additional spectroscopic signatures of electronic doping. (a) The photoluminescence decay dynamics of CdSe nanocrystals change upon *n*-doping (arrows). An extra CB electron ($\langle n_e \rangle < 1$) increases photoluminescence at very short times because of increased radiative transition probabilities and introduces fast nonradiative Auger recombination. Adapted with permission from refs 9 and 27. Copyright 2013 American Chemical Society. (b) EPR *g* values of extra electrons in colloidal *n*-doped ZnO nanocrystals ($\langle n_e \rangle < 1$) depend on nanocrystal volume, confirming delocalization. Adapted with permission from ref 2. Copyright 2008 American Chemical Society.

DOI: 10.1021/acs.accounts.5b00181
Acc. Chem. Res. 2015, 48, 1929−1937

n-type ZnO nanocrystals prepared by photodoping.[2] The *g* value decreases with increasing nanocrystal diameter, asymptotically approaching that of bulk ZnO at large diameters[2,28,29] as anticipated from perturbation theory,[30] confirming electron delocalization over the entire nanocrystal volume. Similar EPR spectra at 4 K confirm that the electrons do not localize into traps.[2] Essentially identical EPR spectra are observed in colloidal *n*-type Al^{3+}-doped ZnO (AZO) nanocrystals.[31] Although delocalized carriers in other nanocrystals should behave similarly, the EPR of quantum-confined carriers has not been extensively studied.

3. ELECTRONIC DOPING AT THERMAL EQUILIBRIUM

3.1. Chemical Reduction and Photodoping

Early investigations of excess band-like carriers in colloidal semiconductor nanocrystals were performed by Henglein and co-workers,[32] who introduced excess electrons into colloidal ZnO nanocrystals by electron transfer from radiolytic free radicals and by photochemical oxidation of alcohols. Both chemistries lead to similar band-edge absorption bleaches, a characteristic of band filling. Band-like electrons were introduced into colloidal ZnO, CdS, and CdSe nanocrystals by Guyot-Sionnest and co-workers via outer-sphere electron transfer using biphenyl radical as a solvated reductant.[33] Intense new intraband absorption in the infrared allowed these authors to definitively conclude the formation of colloidal *n*-type nanocrystals with quantum-confined, delocalized electrons. Numerous subsequent studies have explored the introduction of delocalized charge carriers into colloidal semiconductor nanocrystals at equilibrium conditions by electron-transfer (remote chemical doping, Scheme 2a)[10,17,25,34−38] and photochemical (photodoping, Scheme 2b)[9,22,23,32,39−45] methods.

Scheme 2

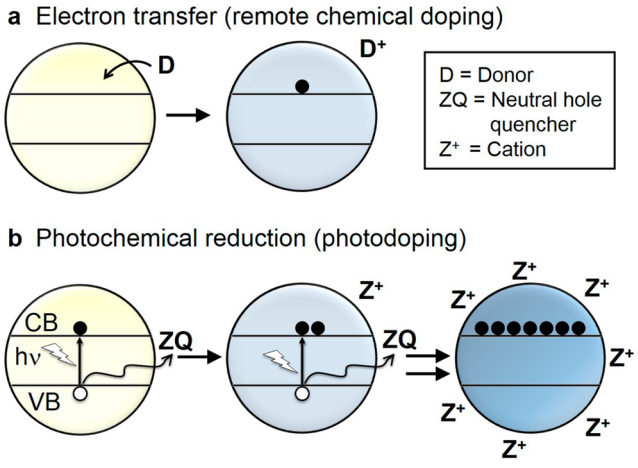

3.2. Defect Doping

Perhaps the most prevalent strategy for semiconductor electronic doping involves the introduction of charged impurities, vacancies, or other defects compensated by excess charge carriers (Scheme 3a). Unlike photodoping or electron-transfer methods, this strategy can yield very stable *n*- or *p*-type nanocrystals that are relatively easy to handle and process. Carrier addition via defect doping has been successful in oxide,[7,15,18,19,22,31,46,47] Si,[16,21] and $Cu_{2-x}E$ (E = S, Se, Te)[12−14,48] nanocrystals but remains a challenge for many

Scheme 3

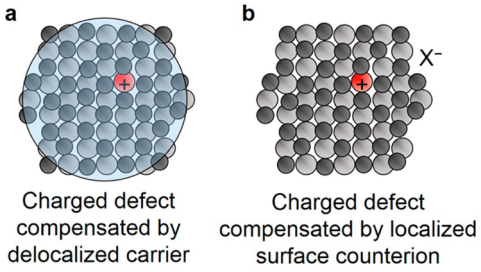

other systems because only rarely do charged defects successfully introduce excess band-like charge carriers. In most cases, charged defects are compensated by localized counter charges at the nanocrystal surfaces, such as from ligands or surface nonstoichiometries (Scheme 3b). For example, in Al^{3+}-doped ZnO (AZO) nanocrystals, only ~5% of Al^{3+} dopants are compensated by CB electrons,[31] and the majority are compensated elsewhere. Surface compensation thus represents a major impediment to nanocrystal electronic doping.

Similarly, only some of the Sn^{4+} cations substituting for In^{3+} in tin-doped In_2O_3 (ITO) nanocrystals are compensated by delocalized CB electrons.[19,22,47] Although the exact origin of these delocalized electrons is unclear, they may come from oxidation of organic reagents during synthesis, because tin is introduced as Sn^{4+} and is thus ionized prior to inclusion in the nanocrystal. Figure 4a shows absorption spectra of colloidal In_2O_3 and ITO nanocrystals containing various amounts of Sn^{4+}.[22] Bleached band-edge and new IR absorption are apparent, consistent with electronic doping as outlined above, and carrier freeze-out is not observed down to liquid He

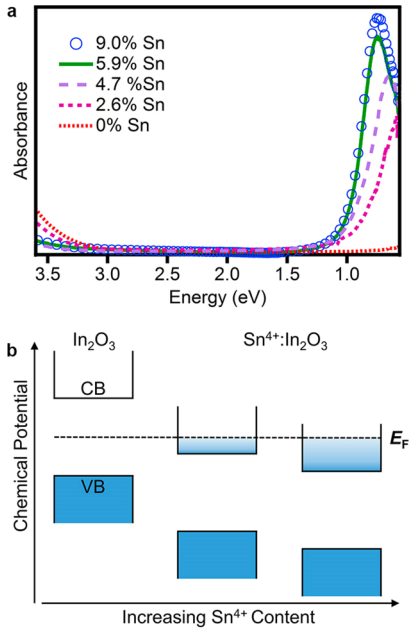

Figure 4. Addition of CB electrons into colloidal In_2O_3 nanocrystals via aliovalent doping with Sn^{4+}. (a) Absorption spectra show loss of band-edge absorption and new IR absorption with Sn^{4+} incorporation. (b) Schematic representation of shifts in the band edges (redox potential) with added Sn^{4+}. Stabilization of the CB edge below E_F allows accumulation of CB electrons. Adapted with permission from ref 22. Copyright 2015 American Chemical Society.

DOI: 10.1021/acs.accounts.5b00181
Acc. Chem. Res. 2015, 48, 1929−1937

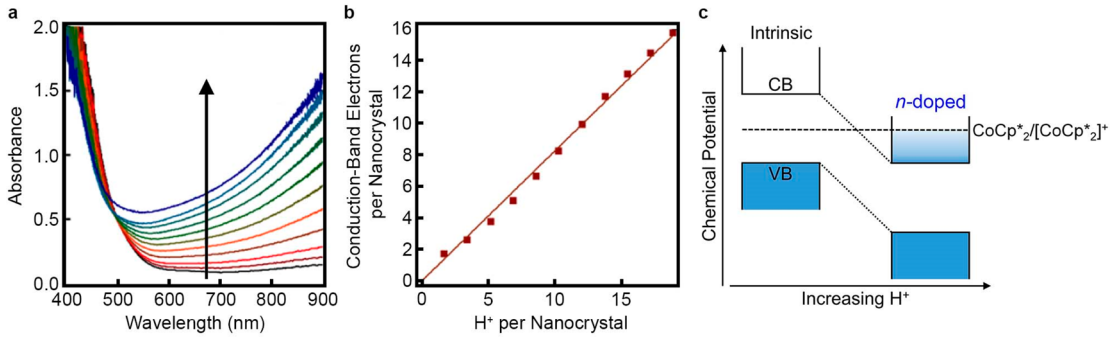

Figure 5. Shifting redox potentials of colloidal ZnO nanocrystals using protons. (a) Absorption spectra of ZnO nanocrystals with 20 equiv of $CoCp^*_2$ and various amounts of added H^+. The arrow shows the direction of increased H^+. (b) Number of CB electrons added per ZnO nanocrystal vs added H^+. Panels a and b adapted with permission from ref 36. Copyright 2013 American Chemical Society. (c) Schematic representation of ZnO nanocrystal band-edge stabilization by H^+.

temperatures,[22] indicating degenerate doping with E_F above the CB edge. In contrast with the electron-transfer and photodoping examples discussed above, these excess electrons are extremely stable, allowing ITO nanocrystals to be handled in air without oxidation. Colloidal AZO nanocrystals show similar stability.[31,49,50]

A striking observation is that ITO nanocrystals do not transfer electrons to undoped In_2O_3 nanocrystals,[22] despite having E_F above their CB edge. In photodoped nanocrystals, rapid electron transfer is observed when a driving force exists.[22,51,52] These observations indicate that rather than raising E_F, Sn^{4+} dopants *stabilize* the In_2O_3 CB relative to E_F (Figure 4b), which is defined by the solution and nanocrystal surfaces. This CB stabilization is due to strong Sn^{4+}−electron Coulomb interactions.

3.3. Equilibrium Charge Injection upon Redox Shifting

It is also possible to shift nanocrystal band-edge potentials using extrinsic ions or surface dipoles. Such postsynthetic redox-potential tuning offers a valuable tool for modifying electronic properties. To illustrate, Figure 5a shows a series of electronic absorption spectra collected during electron-transfer reduction of colloidal ZnO nanocrystals.[36] As-prepared nanocrystals show little intraband absorption even after adding 20 equivalents of the reductant $CoCp^*_2$, indicating little electron transfer. Upon addition of protons, however, electrons are transferred to ZnO. Figure 5b shows a linear relationship between the number of CB electrons added per nanocrystal and proton equivalents,[36] indicating that the electron transfer is gated by protons. Here, the $CoCp^*_2$ redox couple defines E_F for the colloidal solution. Protons shift the ZnO CB lower and, when the electron chemical potential in ZnO is below that in $CoCp^*_2$, equilibrium electron transfer to ZnO is thermodynamically favored. This result is summarized schematically in Figure 5c, which reflects the well-known potential−pH Pourbaix diagrams derived from the Nernst equation[53] and widely observed in bulk and nanoscale oxides.[54−56] A similar phenomenon was recently observed in colloidal HgS nanocrystals,[38] where addition of Hg^{2+} to undoped nanocrystals yielded a band-edge absorption bleach and new intraband absorption, suggesting that Hg^{2+} binding stabilizes the CB sufficiently for nanocrystal reduction, presumably by reduced surface traps.

These examples illustrate the powerful conclusion that postsynthetic redox shifting can generate electronically doped colloidal nanocrystals when performed in the presence of a suitable reservoir of charge carriers. Notably, the added ions (H^+, Hg^{2+}) are not themselves donating the electrons but instead are shifting band-edge potentials such that redox equilibria involving *other* redox-active species favor nanocrystal reduction.

4. REDOX-POTENTIAL TUNING WITHOUT EQUILIBRIUM CHARGE INJECTION

In many cases, semiconductor band edges are shifted without addition of free carriers. Scheme 1c,d illustrates a scenario in which perturbation of a nanocrystal makes it easier to reduce, but E_F is too far from the band edges to introduce substantial concentrations of band-like charge carriers. We categorize such nanocrystals as redox-shifted. In colloids, this scenario shows obvious qualitative differences from the scenarios discussed above. In quantum-dot solids, ensemble carrier types and densities can be altered via such perturbations.[57−61]

4.1. Surface Dipoles

Recent work has demonstrated that tuning dipole moments at colloidal PbS nanocrystal surfaces can shift absolute CB and VB energies substantially (Figure 6).[62] Surface dipoles were interpreted as sums of molecular and interface dipoles, with ligands presumably binding as anions to surface Pb^{2+}. Band-edge energies were measured using UV photoelectron spectroscopy (UPS, Figure 6c). Molecules that withdraw electron density from the nanocrystals stabilize the bands, whereas those that donate electron density destabilize the bands. Even without generating free carriers, surface dipoles clearly impact the electronic properties of the nanocrystals, tuning their redox potentials by over ∼1 V. This type of redox-potential tuning is a powerful capability in the development of nanocrystals for photovoltaics or other electronic applications.

4.2. Ionic Impurities

Another interesting example of redox shifting is seen in InAs nanocrystals exposed to excess cations. InAs nanocrystals containing large numbers of copper or silver impurity ions have been prepared and characterized via scanning tunneling spectroscopy (STS).[63] Figure 7a shows absorption spectra of the parent InAs nanocrystals and of the same nanocrystals after addition of $CuCl_2$, AgCl, or $AgNO_3$. The cations quickly diffuse into the InAs lattice, with their charge-compensating anions likely remaining at the nanocrystal surfaces. These cations cause small shifts of the first excitonic absorption energy but no evident bleaching, indicating negligible free-carrier densities under these conditions. STS data (Figure 7b) show large shifts

DOI: 10.1021/acs.accounts.5b00181
Acc. Chem. Res. 2015, 48, 1929−1937

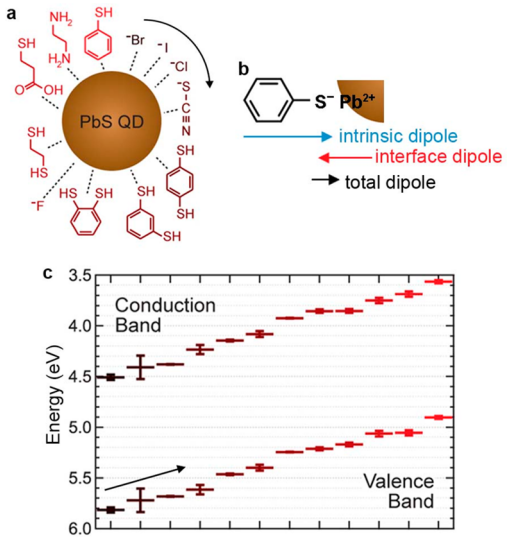

Figure 6. Redox shifting of colloidal PbS nanocrystals via ligand exchange. (a) Schematic representation of the ligands investigated. (b) Total surface dipole, represented as a sum of molecular and interface dipoles. (c) CB and VB energies measured by UPS. The arrow shows the order in which the band energies are given, coinciding with the arrow in panel a progressing clockwise starting with Br^-. Adapted with permission from ref 62. Copyright 2014 American Chemical Society.

of the band energies, however (i.e., redox-potential shifting). Figure 7c depicts these changes schematically. EXAFS data suggest that copper ions are incorporated interstitially,[64] where their positive charges stabilize the InAs CB, making the nanocrystals easier to reduce. Silver is proposed to incorporate substitutionally in its +1 oxidation state.[63] Replacement of In^{3+} with Ag^+ yields a net negative charge that destabilizes the bands, making the nanocrystals more difficult to reduce. In each case, the bands are shifted relative to a reference potential (V_0), but free carriers are introduced only with applied bias, that is, under nonequilibrium conditions. The same shifts in redox potentials should be observable electrochemically, for example, Figure 2.

Redox shifting is also evident in Ag^+-doped CdSe nanocrystals. Figure 8a shows absorption spectra of undoped and Ag^+-doped CdSe colloidal nanocrystals at various Ag^+ concentrations.[59] No excitonic absorption bleach is observed upon Ag^+ addition, again indicating an absence of free carriers. The electronic properties of these Ag^+-doped CdSe nanocrystals were probed by incorporating them into thin-film field-effect transistors (FETs). Figure 8b plots drain current (I_D) vs reference voltage (V) for devices containing nanocrystals with different Ag^+ concentrations. The sharp increase in I_D with increasingly positive V indicates that electrons are the mobile charge carriers in these films. Figure 8c shows that the device turn-on voltage generally becomes more positive as the amount of Ag^+ per nanocrystal increases. Because the band gap does not change with added Ag^+ (Figure 8a), the VB is also shifted, as in Figure 7c (right). These results demonstrate that charged impurities can tune electronic properties of colloidal semiconductor nanocrystals enough to affect device performance, even without introducing free carriers at thermal equilibrium.

5. IMPORTANCE OF CHARGE-CARRIER RESERVOIRS

In the examples of Section 4, excess free carriers are only observed under nonequilibrium conditions, much like in

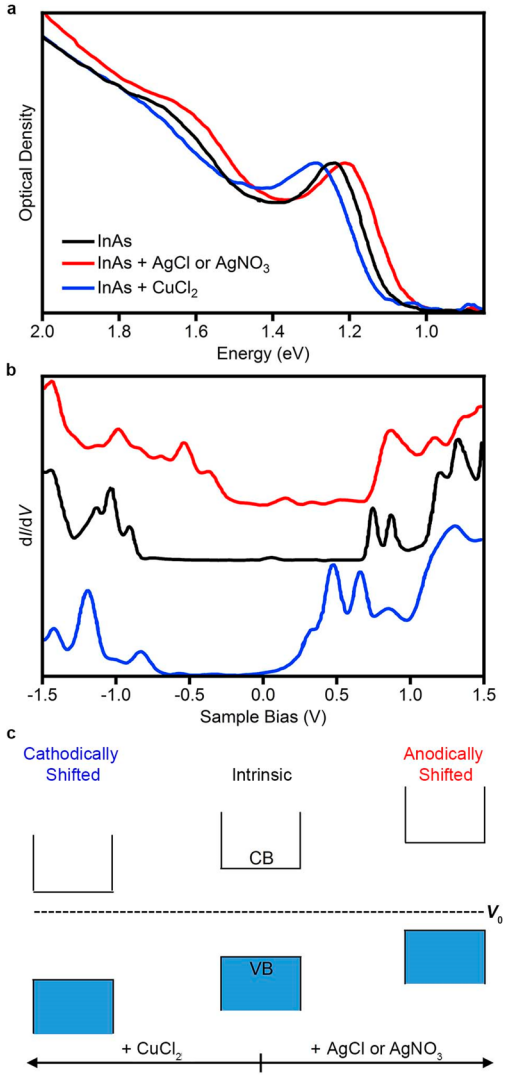

Figure 7. Redox shifting of InAs nanocrystals via addition of cations. (a) Absorption spectra of as-prepared InAs nanocrystals (black) and the same nanocrystals with added $AgNO_3$ (red) or $CuCl_2$ (blue). (b) STM spectra of the nanocrystals from panel a. Panels a and b adapted with permission from ref 63. Copyright 2011 AAAS. (c) Schematic summary of the shifts in band-edge potentials with ion addition.

intrinsic nanocrystals. The question arises: Why are equilibrium free-carrier populations observed in some cases (Figures 1, 4, and 5) but not others (Figures 6–8)? When aliovalent dopants are added (e.g., Sn^{4+} into In_2O_3, Ag^+ into InAs or CdSe), they are typically already ionized and hence cannot themselves provide the charge-compensating carriers. The appearance of excess free carriers is thus limited not just by nanocrystal composition, but also by the availability of charge-carrier reservoirs with suitable potentials, for example, solvated redox reagents or redox-active surface species (traps, vacancies, etc.). Given such a reservoir, the chemical potential of a carrier within the nanocrystal then must be tuned relative to that of the reservoir to achieve equilibrium carrier transfer into a nanocrystal band. In Figures 6–8, no such reservoirs are evidently available. In many cases, the availability of a suitable carrier reservoir is intimately linked to the redox potentials of nanocrystal surface traps (Scheme 1c). Without controlling surfaces, E_F is poorly defined and likely poorly positioned, and electronic doping chemistries will be similarly poorly

DOI: 10.1021/acs.accounts.5b00181
Acc. Chem. Res. 2015, 48, 1929–1937

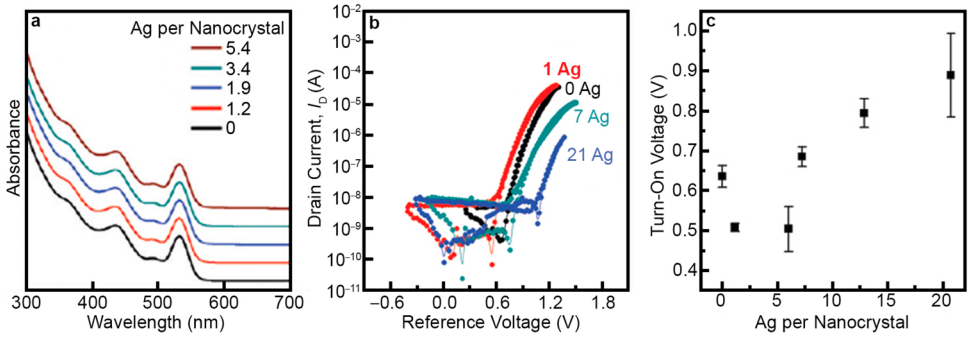

Figure 8. Effects of Ag^+ doping on CdSe nanocrystal-based devices. (a) Absorption spectra of colloidal CdSe nanocrystals with various amounts of Ag^+. (b) FET measurements on quantum-dot-film devices made with CdSe nanocrystals containing various amounts of Ag^+. (c) FET turn-on voltages as a function of added Ag^+. Adapted with permission from ref 59. Copyright 2012 American Chemical Society.

controlled. In addition to the many synthetic challenges associated with composition control (not addressed here), future progress in nanocrystal electronic doping therefore requires improved understanding and control of surface chemistries at the microscopic level. Recent advances in this direction are encouraging.[65,66]

6. CONCLUSION

The preparation of electronically doped colloidal semiconductor nanocrystals possessing excess band-like charge carriers at thermal equilibrium represents a long-standing challenge in nanoscience, with ramifications for both fundamental research and numerous potential technologies. This Account highlights several recent successes in this field. A distinction is proposed between electronic doping that introduces equilibrium excess band-like charge carriers and electrostatic redox-potential shifting without equilibrium excess band-like charge carriers. Spectroscopic signatures are outlined for distinguishing between these two regimes experimentally. Future advances in controlling nanocrystal compositions, surface chemistries, and redox reactivities will undoubtedly yield a diverse portfolio of new materials with attractive physical and electronic properties that will accelerate the development of nanocrystal-based technologies.

AUTHOR INFORMATION

Corresponding Author

*E-mail: gamelin@chem.washington.edu.

Funding

Financial support from the U.S. National Science Foundation (Grants CHE-1151726 and DMR-1206221) is gratefully acknowledged. A.M.S. thanks the NSF-GRFP and the UW Clean Energy Institute for funding. K.E.K. is supported by DOE-EERE.

Notes

The authors declare no competing financial interest.

Biographies

Alina M. Schimpf received her Ph.D. in 2014 with Prof. Daniel Gamelin at the University of Washington. Her research focused on the study of electronically doped and impurity-doped colloidal semiconductor nanocrystals. Alina received an NSF Graduate Research Fellowship and a University of Washington Clean Energy Institute Exploratory Research Fellowship. She is currently a postdoctoral associate with Prof. Mircea Dincă at Massachusetts Institute of Technology.

Kathryn E. Knowles completed her Ph.D. at Northwestern University in 2013 as a DOE Office of Science Graduate Research Fellow studying the effects of surface chemistry on the optical and electronic properties of colloidal nanocrystals under the guidance of Prof. Emily Weiss. She is now a postdoctoral researcher in Prof. Gamelin's group studying copper-doped colloidal nanocrystals with the support of a DOE Energy Efficiency and Renewable Energy (EERE) Postdoctoral Research Award.

Gerard M. Carroll received his B.S. in Chemistry from Fort Lewis College and is currently working toward his Ph.D. at the University of Washington with Prof. Daniel Gamelin. He studies the effects of interfaces on the electronic, redox, and catalytic properties of semiconductors. He is the recipient of the Rowland Endowed Fellowship in Chemistry.

Daniel R. Gamelin holds the Harry and Catherine Jaynne Boand Endowed Professorship in Chemistry at the University of Washington, Seattle, where he has been on the faculty since 2000. His research involves the development and investigation of new inorganic materials with unusual electronic structures that give rise to desirable photophysical, photochemical, magnetic, or magneto-optical properties. He is a Fellow of the American Association for the Advancement of Science, an associate editor for *Chemical Communications* (Royal Society of Chemistry), and the 2015 ACS Inorganic Chemistry Lectureship Awardee.

REFERENCES

(1) Kittel, C. *Introduction to Solid State Physics*, 8 ed.; Wiley: New York, 2004.
(2) Whitaker, K. M.; Ochsenbein, S. T.; Polinger, V. Z.; Gamelin, D. R. Electron Confinement Effects in the EPR Spectra of Colloidal n-Type ZnO Quantum Dots. *J. Phys. Chem. C* **2008**, *112*, 14331−14335.
(3) Schimpf, A. M.; Thakkar, N.; Gunthardt, C. E.; Masiello, D. J.; Gamelin, D. R. Charge-Tunable Quantum Plasmons in Colloidal Semiconductor Nanocrystals. *ACS Nano* **2013**, *8*, 1065−1072.
(4) Kumar, C. P.; Gopal, N. O.; Wang, T. C.; Wong, M.-S.; Ke, S. C. EPR Investigation of TiO_2 Nanoparticles with Temperature-Dependent Properties. *J. Phys. Chem. B* **2006**, *110*, 5223−5229.
(5) Fittipaldi, M.; Curri, M. L.; Comparelli, R.; Striccoli, M.; Agostiano, A.; Grassi, N.; Sangregorio, C.; Gatteschi, D. A Multifrequency EPR Study on Organic-Capped Anatase TiO_2 Nanocrystals. *J. Phys. Chem. C* **2009**, *113*, 6221−6226.
(6) Chiesa, M.; Paganini, M. C.; Livraghi, S.; Giamello, E. Charge Trapping in TiO_2 Polymorphs as Seen by Electron Paramagnetic Resonance Spectroscopy. *Phys. Chem. Chem. Phys.* **2013**, *15*, 9435−9447.

DOI: 10.1021/acs.accounts.5b00181
Acc. Chem. Res. 2015, 48, 1929−1937

(7) De Trizio, L.; Buonsanti, R.; Schimpf, A. M.; Llordes, A.; Gamelin, D. R.; Simonutti, R.; Milliron, D. J. Nb-Doped Colloidal TiO_2 Nanocrystals with Tunable Infrared Absorption. *Chem. Mater.* **2013**, *25*, 3383−3390.
(8) Reiss, H. The Fermi Level and the Redox Potential. *J. Phys. Chem.* **1985**, *89*, 3783−3791.
(9) Rinehart, J. D.; Schimpf, A. M.; Weaver, A. L.; Cohn, A. W.; Gamelin, D. R. Photochemical Electronic Doping of Colloidal CdSe Nanocrystals. *J. Am. Chem. Soc.* **2013**, *135*, 18782−18785.
(10) Shim, M.; Wang, C.; Guyot-Sionnest, P. Charge-Tunable Optical Properties in Colloidal Semiconductor Nanocrystals. *J. Phys. Chem. B* **2001**, *105*, 2369−2373.
(11) Kanehara, M.; Koike, H.; Yoshinaga, T.; Teranishi, T. Indium Tin Oxide Nanoparticles with Compositionally Tunable Surface Plasmon Resonance Frequencies in the Near-IR Region. *J. Am. Chem. Soc.* **2009**, *131*, 17736−17737.
(12) Zhao, Y.; Pan, H.; Lou, Y.; Qiu, X.; Zhu, J.; Burda, C. Plasmonic $Cu_{2-x}S$ Nanocrystals: Optical and Structural Properties of Copper-Deficient Copper(I) Sulfides. *J. Am. Chem. Soc.* **2009**, *131*, 4253−4261.
(13) Luther, J.; Jain, P.; Ewers, T.; Alivisatos, A. Localized Surface Plasmon Resonances Arising from Free Carriers in Doped Quantum Dots. *Nat. Mater.* **2011**, *10*, 361−366.
(14) Dorfs, D.; Härtling, T.; Miszta, K.; Bigall, N. C.; Kim, M. R.; Genovese, A.; Falqui, A.; Povia, M.; Manna, L. Reversible Tunability of the Near-Infrared Valence Band Plasmon Resonance in $Cu_{2-x}Se$ Nanocrystals. *J. Am. Chem. Soc.* **2011**, *133*, 11175−11180.
(15) Manthiram, K.; Alivisatos, A. Tunable Localized Surface Plasmon Resonances in Tungsten Oxide Nanocrystals. *J. Am. Chem. Soc.* **2012**, *134*, 3995−3998.
(16) Rowe, D. J.; Jeong, J. S.; Mkhoyan, K. A.; Kortshagen, U. R. Phosphorus-Doped Silicon Nanocrystals Exhibiting Mid-Infrared Localized Surface Plasmon Resonance. *Nano Lett.* **2013**, *13*, 1317−1322.
(17) Palomaki, P. K. B.; Miller, E. M.; Neale, N. R. Control of Plasmonic and Interband Transitions in Colloidal Indium Nitride Nanocrystals. *J. Am. Chem. Soc.* **2013**, *135*, 14142−14150.
(18) Diroll, B. T.; Gordon, T. R.; Gaulding, E. A.; Klein, D. R.; Paik, T.; Yun, H. J.; Goodwin, E. D.; Damodhar, D.; Kagan, C. R.; Murray, C. B. Synthesis of n-Type Plasmonic Oxide Nanocrystals and the Optical and Electrical Characterization of their Transparent Conducting Films. *Chem. Mater.* **2014**, *26*, 4579−4588.
(19) Lounis, S. D.; Runnerstrom, E. L.; Bergerud, A.; Nordlund, D.; Milliron, D. J. Influence of Dopant Distribution on the Plasmonic Properties of Indium Tin Oxide Nanocrystals. *J. Am. Chem. Soc.* **2014**, *136*, 7110−7116.
(20) Ye, X.; Fei, J.; Diroll, B. T.; Paik, T.; Murray, C. B. Expanding the Spectral Tunability of Plasmonic Resonances in Doped Metal-Oxide Nanocrystals through Cooperative Cation−Anion Codoping. *J. Am. Chem. Soc.* **2014**, *136*, 11680−11686.
(21) Zhou, S.; Pi, X.; Ni, Z.; Ding, Y.; Jiang, Y.; Jin, C.; Delerue, C.; Yang, D.; Nozaki, T. Comparative Study on the Localized Surface Plasmon Resonance of Boron- and Phosphorus-Doped Silicon Nanocrystals. *ACS Nano* **2015**, *9*, 378−386.
(22) Schimpf, A. M.; Runnerstrom, E. L.; Lounis, S. D.; Milliron, D. J.; Gamelin, D. R. Redox Energies and Plasmon Resonance Energies of Photodoped In_2O_3 and Sn-doped In_2O_3 Nanocrystals. *J. Am. Chem. Soc.* **2015**, *137*, 518−524.
(23) Faucheaux, J. A.; Jain, P. K. Plasmons in Photocharged ZnO Nanocrystals Revealing the Nature of Charge Dynamics. *J. Phys. Chem. Lett.* **2013**, *4*, 3024−3030.
(24) Wehrenberg, B. L.; Guyot-Sionnest, P. Electron and Hole Injection in PbSe Quantum Dot Films. *J. Am. Chem. Soc.* **2003**, *125*, 7806−7807.
(25) Koh, W.-K.; Koposov, A. Y.; Stewart, J. T.; Pal, B. N.; Robel, I.; Pietryga, J. M.; Klimov, V. I. Heavily Doped n-Type PbSe and PbS Nanocrystals Using Ground-State Charge Transfer from Cobaltocene. *Sci. Rep.* **2013**, *3*, No. 2004.
(26) Liu, H.; Keuleyan, S.; Guyot-Sionnest, P. n- and p-Type HgTe Quantum Dot Films. *J. Phys. Chem. C* **2011**, *116*, 1344−1349.
(27) Cohn, A. W.; Schimpf, A. M.; Gunthardt, C. E.; Gamelin, D. R. Size-Dependent Trap-Assisted Auger Recombination in Semiconductor Nanocrystals. *Nano Lett.* **2013**, *13*, 1810−1815.
(28) Orlinskii, S. B.; Blok, H.; Schmidt, J.; Baranov, P. G.; de Mello Donegá, C.; Meijerink, A. Donor-Acceptor Pairs in the Confined Structure of ZnO Nanocrystals. *Phys. Rev. B* **2006**, *74*, No. 045204.
(29) Zhou, H.; Hofstaetter, A.; Hofmann, D. M.; Meyer, B. K. Magnetic Resonance Studies on ZnO Nanocrystals. *Microelectron. Eng.* **2003**, *66*, 59−64.
(30) Rodina, A. V.; Efros, A. L.; Rosen, M.; Meyer, B. K. Theory of the Zeeman Effect in Semiconductor Nanocrystals. *Mater. Sci. Eng., C* **2002**, *19*, 435−438.
(31) Schimpf, A. M.; Ochsenbein, S. T.; Buonsanti, R.; Milliron, D. J.; Gamelin, D. R. Comparison of Extra Electrons in Colloidal *n*-type Al^{3+}-Doped and Photochemically Reduced ZnO Nanocrystals. *Chem. Commun.* **2012**, *48*, 9352−9354.
(32) Haase, M.; Weller, H.; Henglein, A. Photochemistry and Radiation Chemistry of Colloidal Semiconductors. 23. Electron Storage on ZnO Particles and Size Quantization. *J. Phys. Chem.* **1988**, *92*, 482−487.
(33) Shim, M.; Guyot-Sionnest, P. n-Type Colloidal Semiconductor Nanocrystals. *Nature* **2000**, *407*, 981−983.
(34) Wang, C. J.; Shim, M.; Guyot-Sionnest, P. Electrochromic Nanocrystal Quantum Dots. *Science* **2001**, *291*, 2390−2392.
(35) Yu, D.; Wang, C.; Guyot-Sionnest, P. n-Type Conducting CdSe Nanocrystal Solids. *Science* **2003**, *300*, 1277−1280.
(36) Valdez, C. N.; Braten, M.; Soria, A.; Gamelin, D. R.; Mayer, J. M. Effect of Protons on the Redox Chemistry of Colloidal Zinc Oxide Nanocrystals. *J. Am. Chem. Soc.* **2013**, *135*, 8492−8495.
(37) Wheeler, L. M.; Neale, N. R.; Chen, T.; Kortshagen, U. R. Hypervalent Surface Interactions for Colloidal Stability and Doping of Silicon Nanocrystals. *Nat. Commun.* **2013**, *4*, No. 2197.
(38) Jeong, K. S.; Deng, Z.; Keuleyan, S.; Liu, H.; Guyot-Sionnest, P. Air-Stable n-Doped Colloidal HgS Quantum Dots. *J. Phys. Chem. Lett.* **2014**, *5*, 1139−1143.
(39) Wood, A.; Giersig, M.; Mulvaney, P. Fermi Level Equilibration in Quantum Dot-Metal Nanojunctions. *J. Phys. Chem. B* **2001**, *105*, 8810−8815.
(40) Shim, M.; Guyot-Sionnest, P. Organic-Capped ZnO Nanocrystals: Synthesis and n-Type Character. *J. Am. Chem. Soc.* **2001**, *123*, 11651−11654.
(41) Germeau, A.; Roest, A. L.; Vanmaekelbergh, D.; Allan, G.; Delerue, C.; Meulenkamp, E. A. Optical Transitions in Artificial Few-Electron Atoms Strongly Confined Inside ZnO Nanocrystals. *Phys. Rev. Lett.* **2003**, *90*, No. 097401.
(42) Liu, W. K.; Whitaker, K. M.; Kittilstved, K. R.; Gamelin, D. R. Stable Photogenerated Carriers in Magnetic Semiconductor Nanocrystals. *J. Am. Chem. Soc.* **2006**, *128*, 3910−3911.
(43) Liu, W. K.; Whitaker, K. M.; Smith, A. L.; Kittilstved, K. R.; Robinson, B. H.; Gamelin, D. R. Room-Temperature Electron Spin Dynamics in Free-Standing ZnO Quantum Dots. *Phys. Rev. Lett.* **2007**, *98*, No. 186804.
(44) Cohn, A. W.; Janßen, N.; Mayer, J. M.; Gamelin, D. R. Photocharging ZnO Nanocrystals: Picosecond Hole Capture, Electron Accumulation, and Auger Recombination. *J. Phys. Chem. C* **2012**, *116*, 20633−20642.
(45) Schimpf, A. M.; Gunthardt, C. E.; Rinehart, J. D.; Mayer, J. M.; Gamelin, D. R. Controlling Carrier Densities in Photochemically Reduced Colloidal ZnO Nanocrystals: Size Dependence and Role of the Hole Quencher. *J. Am. Chem. Soc.* **2013**, *135*, 16569−16577.
(46) Liang, X.; Ren, Y.; Bai, S.; Zhang, N.; Dai, X.; Wang, X.; He, H.; Jin, C.; Ye, Z.; Chen, Q.; Chen, L.; Wang, J.; Jin, Y. Colloidal Indium-Doped Zinc Oxide Nanocrystals with Tunable Work Function: Rational Synthesis and Optoelectronic Applications. *Chem. Mater.* **2014**, *26*, 5169−5178.

DOI: 10.1021/acs.accounts.5b00181
Acc. Chem. Res. 2015, 48, 1929−1937

(47) Wang, T.; Radovanovic, P. V. Free Electron Concentration in Colloidal Indium Tin Oxide Nanocrystals Determined by Their Size and Structure. *J. Phys. Chem. C* **2011**, *115*, 406−413.
(48) Xie, Y.; Riedinger, A.; Prato, M.; Casu, A.; Genovese, A.; Guardia, P.; Sottini, S.; Sangregorio, C.; Miszta, K.; Ghosh, S.; Pellegrino, T.; Manna, L. Copper Sulfide Nanocrystals with Tunable Composition by Reduction of Covellite Nanocrystals with Cu^{+} Ions. *J. Am. Chem. Soc.* **2013**, *135*, 17630−17637.
(49) Buonsanti, R.; Llordes, A.; Aloni, S.; Helms, B.; Milliron, D. Tunable Infrared Absorption and Visible Transparency of Colloidal Aluminum-Doped Zinc Oxide Nanocrystals. *Nano Lett.* **2011**, *11*, 4706−4716.
(50) Herklotz, F.; Lavrov, E. V.; Weber, J.; Mamin, G. V.; Kutin, Y. S.; Volodin, M. A.; Orlinskii, S. B. Identification of Shallow Al Donors in ZnO. *Phys. Status Solidi B* **2011**, *248*, 1532−1537.
(51) Hayoun, R.; Whitaker, K. M.; Gamelin, D. R.; Mayer, J. M. Electron Transfer Between Colloidal ZnO Nanocrystals. *J. Am. Chem. Soc.* **2011**, *133*, 4228−4231.
(52) Cohn, A. W.; Kittilstved, K. R.; Gamelin, D. R. Tuning the Potentials of "Extra" Electrons in Colloidal *n*-Type ZnO Nanocrystals via Mg^{2+} Substitution. *J. Am. Chem. Soc.* **2012**, *134*, 7937−7943.
(53) Pourbaix, M. *Atlas of Electrochemical Equilibria in Aqueous Solutions*, 2 ed.; National Association of Corrosion Engineers: Houston, TX, 1974.
(54) Bolts, J. M.; Wrighton, M. S. Correlation of Photocurrent-Voltage Curves with Flat-Band Potential for Stable Photoelectrodes for the Photoelectrolysis of Water. *J. Phys. Chem.* **1976**, *80*, 2641−2645.
(55) Duonghong, D.; Ramsden, J.; Grätzel, M. Dynamics of Interfacial Electron-Transfer Processes in Colloidal Semiconductor Systems. *J. Am. Chem. Soc.* **1982**, *104*, 2977−2985.
(56) Ward, M. D.; White, J. R.; Bard, A. J. Electrochemical Investigation of the Energetics of Particulate Titanium Dioxide Photocatalysts. The Methyl Viologen-Acetate System. *J. Am. Chem. Soc.* **1983**, *105*, 27−31.
(57) Geyer, S. M.; Allen, P. M.; Chang, L.-Y.; Wong, C. R.; Osedach, T. P.; Zhao, N.; Bulovic, V.; Bawendi, M. G. Control of the Carrier Type in InAs Nanocrystal Films by Predeposition Incorporation of Cd. *ACS Nano* **2010**, *4*, 7373−7378.
(58) Zhitomirsky, D.; Furukawa, M.; Tang, J.; Stadler, P.; Hoogland, S.; Voznyy, O.; Liu, H.; Sargent, E. H. N-Type Colloidal-Quantum-Dot Solids for Photovoltaics. *Adv. Mater.* **2012**, *24*, 6181−6185.
(59) Sahu, A.; Kang, M. S.; Kompch, A.; Notthoff, C.; Wills, A. W.; Deng, D.; Winterer, M.; Frisbie, C. D.; Norris, D. J. Electronic Impurity Doping in CdSe Nanocrystals. *Nano Lett.* **2012**, *12*, 2587−2594.
(60) Kang, M. S.; Sahu, A.; Frisbie, C. D.; Norris, D. J. Influence of Silver Doping on Electron Transport in Thin Films of PbSe Nanocrystals. *Adv. Mater.* **2013**, *25*, 725−731.
(61) Oh, S. J.; Berry, N. E.; Choi, J.-H.; Gaulding, E. A.; Lin, H.; Paik, T.; Diroll, B. T.; Muramoto, S.; Murray, C. B.; Kagan, C. R. Designing High-Performance PbS and PbSe Nanocrystal Electronic Devices through Stepwise, Post-Synthesis, Colloidal Atomic Layer Deposition. *Nano Lett.* **2014**, *14*, 1559−1566.
(62) Brown, P. R.; Kim, D.; Lunt, R. R.; Zhao, N.; Bawendi, M. G.; Grossman, J. C.; Bulović, V. Energy Level Modification in Lead Sulfide Quantum Dot Thin Films through Ligand Exchange. *ACS Nano* **2014**, *8*, 5863−5872.
(63) Mocatta, D.; Cohen, G.; Schattner, J.; Millo, O.; Rabani, E.; Banin, U. Heavily Doped Semiconductor Nanocrystal Quantum Dots. *Science* **2011**, *332*, 77−81.
(64) Amit, Y.; Fasut, A.; Milo, O.; Rabani, E.; Frenkel, A.; Banin, U. How to Dope a Semiconductor Nanocrystal. *ECS Trans.* **2013**, *58*, 127−133.
(65) Zhitomirsky, D.; Voznyy, O.; Levina, L.; Hoogland, S.; Kemp, K. W.; Ip, A. H.; Thon, S. M.; Sargent, E. H. Engineering Colloidal Quantum Dot Solids Within and Beyond the Mobility-Invariant Regime. *Nat. Commun.* **2014**, *5*, No. 3803.
(66) Owen, J. The Coordination Chemistry of Nanocrystal Surfaces. *Science* **2015**, *347*, 615−616.

DOI: 10.1021/acs.accounts.5b00181
Acc. Chem. Res. 2015, 48, 1929−1937